Catalysis Today 147 (2009) 158–165

Contents lists available at ScienceDirect

Catalysis Today

journal homepage: www.elsevier.com/locate/cattod

Preparation and characterization of carbon nanotube-promoted Co–Cu catalyst for higher alcohol synthesis from syngas

Xin Dong [a], Xue-Lian Liang [a], Hai-Yan Li [a], Guo-Dong Lin [a], Peng Zhang [b], Hong-Bin Zhang [a,*]

[a] Department of Chemistry, College of Chemistry and Chemical Engineering, State Key Laboratory of Physical Chemistry for Solid Surfaces and National Engineering Laboratory for Green Chemical Productions of Alcohols, Ethers and Esters, Xiamen University, Xiamen 361005, China
[b] Department of Chemistry, New Mexico Tech, Socorro, NM 87801, USA

ARTICLE INFO

Article history:
Available online 15 January 2009

Keywords:
Multiwalled carbon nanotubes
CoCu-based catalyst
Higher alcohol synthesis

ABSTRACT

A cobalt–copper catalyst promoted by "herringbone-type" multiwalled carbon nanotubes (CNTs) was developed. This catalyst displayed excellent performance for higher alcohol synthesis (HAS) from syngas, with the (C_{2-8}-alc. + DME)-STY reached 760 mg/(g·h) under the reaction conditions of 5.0 MPa and 573 K, which was 1.78 times that of the CNT-free host, Co_3Cu_1. The addition of a minor amount of the CNTs to the Co_3Cu_1 host did not cause a marked change in apparent activation energy for the HAS, but led to an increase at the surface of the catalyst of the concentration of catalytically active Co-species, CoO(OH), a kind of surface Co-species related closely to the selective formation of the higher alcohols. Excellent adsorption performance of this kind of CNTs for H_2 generated a surface micro-environment with a high concentration of H-adspecies on the functioning catalyst, thus increasing the rate of surface hydrogenation reactions in the HAS. Moreover, synergistic action of the high surface-concentration H-adspecies with CO_2 in the feed-gas led to a greater inhibition for the WGS side-reaction. All these factors contribute considerably to an increase in the yield of alcohols.

1. Introduction

Multiwalled carbon nanotubes (simplified as CNTs in later text) have been drawing increasing attention [1–3] since their discovery [4]. This new form of carbon is structurally close to hollow graphite fiber, except that it has a much higher degree of structural perfection. This kind of nanotube-C possesses several unique features, such as highly graphitized tube-wall, nanosized channel and sp^2-C-constructed surface. They also display exceptionally high mechanical strength, high thermal/electrical conductivity, medium to high specific surface areas, and excellent performance for adsorption and spillover of hydrogen, which render this kind of nanostructured carbon materials full of promise as a novel catalyst promoter. The catalytic studies conducted so far on carbon nanotube-based systems range from selective hydrogenation [5,6], hydrofomylation of alkenes [7], selective dehydrogenation [8], selective oxidation [9], ammonia synthesis [10], Fischer–Tropsch synthesis [11], to methanol synthesis [12,13] and higher alcohol synthesis (simplified as HAS in later text) [14–17], etc. They have shown promising results in terms of activity and selectivity.

The higher alcohols (C_{2+}-alcohols) and dimethyl ether (DME) have been considered as the most important species among coal-based clean synthetic fuels and chemical feedstocks. These C_{2+}-oxygenates have been confirmed to be a better and cleaner automobile fuel with high octane number, and lower emissions of NO_x, ozone, CO, and aromatic vapors [18]. Recently, methyl *tert*-butyl ether (MTBE) as additive of oil-based fuel has been prohibited to be used in some countries or regions due to the new environmental regulation, which has greatly renewed the interest in hydrogenation of syngas to the C_{2+}-oxygenates as gasoline blends.

HAS on the Cu-modified Fischer–Tropsch catalysts based on Co, Fe, or Ni has been extensively studied since the late 1970s. A number of pioneer work and excellent reviews [19–24] have been published on this subject. Progress in this field has considerably contributed to the growing understanding of the nature of these catalytic reaction systems. Nevertheless, the existing technology of HAS is still on a small scale. The single-pass-conversion of the feed-syngas and selectivity to C_{2+}-alcohols are both relatively low. Under the typical reaction conditions, most systems produce methanol (e.g., over alkali-promoted MoS_2 catalysts) or hydrocarbons (e.g., over modified Fischer–Tropsch catalysts) as the main product instead of C_{2+}-alcohols [23–27]. Development of catalyst with high efficiency and selectivity for HAS has been one of the key objectives for R&D efforts.

* Corresponding author. Tel.: +86 592 2184591; fax: +86 592 2184591.
E-mail addresses: pzhang@nmt.edu (P. Zhang), hbzhang@xmu.edu.cn (H.-B. Zhang).

0920-5861/$ – see front matter © 2008 Elsevier B.V. All rights reserved.
doi:10.1016/j.cattod.2008.11.025

Recently, with a kind of home-made CNTs as the promoter, a CNT-promoted Co–Cu catalyst for HAS from syngas has been developed in our lab. We had previously reported the preliminary results on development of this catalyst [14,15]. In this article, preparation of the CNT-promoted Co–Cu catalysts and their catalytic performance for HAS from syngas were reported in detail. By means of a series of physico-chemical methods, the texture, structure and properties of the catalysts were characterized, and the nature of promoter action by this kind of CNTs was discussed. The results shed some light on the understanding of the mechanism of promoter action by the CNT-additive and on the design of catalyst for the HAS.

2. Experimental

2.1. Preparation of CNTs and CNT-promoted Co–Cu catalysts

The used CNTs were synthesized according to the previously reported method [28] by catalytic decomposition of CH_4 or CO on a Ni–Mg–O catalyst. The produced CH_4-derived and CO-derived CNTs were a kind of "herringbone-type" CNTs (symbolized as CNTs(*h-type*) or simplified as CNTs in later text) and a kind of "parallel-type" CNTs (symbolized as CNTs(*p-type*) in later text), respectively [29,30]. The freshly prepared CNTs were twice treated with boiling concentrated nitric acid for 4 h, followed by rinsing with de-ionized water, and then drying at 473 K under dried nitrogen. Open-end CNTs with hydrophilic surface were thus obtained.

Using the above home-made CNTs and the nitrates of the corresponding metallic components, a series of CNT-promoted Co–Cu catalysts, denoted as Co_iCu_j–*x*%CNT (where *x*% represented mass percentage), were prepared by constant-pH co-precipitation method. An aqueous solution containing calculated amounts of Co and Cu (total equivalent concentration of metallic cations at 4 N), which was prepared by dissolving $Co(NO_3)_2{\cdot}6H_2O$ and $Cu(NO_3)_2{\cdot}3H_2O$ (all of AR grade) in deionized water, and an aqueous K_2CO_3 solution (4 N) were simultaneously added dropwise under vigorous stirring into a Pyrex flask containing a calculated amount of the HNO_3-treated CNTs at constant temperature of 353 K. The addition was adjusted to maintain a constant pH of around 7. The precipitation process was completed in 1 h. The precipitate was then continuously stirred for 5 h under the temperature of 353 K, followed by aging overnight at room temperature and then filtering. It was then rinsed several times with deionized water until the content of K^+ ions in the eluant fell below 1 ppm, as detected by flame ion absorption method. The precipitate was then dried at 393 K for 4 h and calcined at 543–573 K for 3 h to yield the precursor of CNT-promoted Co–Cu catalysts. A CNTs(*p-type*)-promoted Co–Cu catalyst and an AC (activated carbon)-doped Co–Cu catalyst, as well as a CNT-free conventional co-precipitated Co–Cu catalyst, all used as references, were prepared in the similar way. All samples of catalyst precursor were pressed, crushed, and sieved to a size of 40–80 mesh for the activity evaluation.

2.2. Catalyst evaluation

Performance of the catalysts for the HAS from syngas was evaluated in a fixed-bed continuous-flow reactor and gas chromatograph (GC) combination system. 0.50 g of catalyst (equivalent to approximately 0.5 ml of catalyst sample) was used for each test. Prior to the reaction, the sample of the oxide-precursor of catalyst was pre-reduced *in situ* by a N_2-carried 5%H_2 gaseous mixture for 16 h. HAS from syngas was conducted at a stationary state with pre-mixed feed-gas composition of $V(H_2)/V(CO)/V(CO_2)/V(N_2)$ = 60/30/5/5 or 45/45/5/5 or $V(H_2)/V(CO)/V(N_2)$ = 45/45/10 under 5.0 MPa, 523–583 K. Exit gas from the reactor was immediately brought down to atmospheric pressure and transported, while maintaining temperature at 403 K, to the sampling valve of GC (Model GC-950 by Shanghai Haixin GC Instruments, Inc.), which was equipped with dual detectors (TCD and FID) and dual columns filled with carbon molecular sieve (TDX-01) and Porapak Q-S (USA), respectively, for on-line analysis. The former column (2.0 m length) was used for the analysis of N_2 (as an internal standard), CO and CO_2, and the latter (2.0 m length) for hydrocarbons, alcohols and other oxygenates (mainly DME and acetaldehyde in a small amount). CO conversion (simplified as *X*(CO)) was determined through the internal standard (N_2), and the carbon-based selectivity for the carbon-containing products, including alcohols, hydrocarbons, and other oxygenates (simplified as *S*(alc.), *S*(HC), etc. in later text) was calculated by an internal normalization method.

2.3. Catalyst characterization

Scanning electron microscope (SEM) and high-resolution transmission electron microscope (HRTEM) imagings were performed on LEO-1530 (LEO, Germany) and Technai F30 (Philips, The Netherlands) electron microscopes, respectively. X-ray diffraction measurements were carried out on a Rigaku Rotaflex D/Max-C X-ray diffractometer with Cu Kα radiation at a scanning rate of 8°/min. X-ray photoelectron spectroscopy (XPS) measurements were done on a Quantum 2000 Scanning ESCA Microprobe machine (PHI, USA) with Al Kα radiation (15 kV, 25 W, $h\nu$ = 1486.6 eV) under ultrahigh vacuum (10^{-7} Pa), calibrated internally by carbon deposit C(1s) (E_b = 284.6 eV). Specific surface area (SSA) of the CNTs and catalyst samples was determined by N_2 adsorption using a Micromeritics Tristar-3000 (Carlo Erba) system.

Tests of H_2-temperature-programmed desorption (TPD) of catalyst were conducted on a combined fixed-bed continuous-flow reactor and adsorption–desorption system. The rate of temperature increase was 10 K/min. Change of hydrogen-signal was monitored using an on-line GC (Shimadzu GC-8A) with a thermal conductivity detector (TCD). 100 mg of catalyst sample was used for each run. Prior to the TPD measurement, the catalyst sample was pre-reduced *in situ* in the TPD equipment by the N_2-carried 5%H_2 gaseous mixture stream (40 ml/min), with the highest reduction-temperature reaching 573 K and lasting for 16 h. The reduced sample was cooled to 433 K, followed by switching to a H_2 (of 99.999% purity) stream and maintaining at 433 K for 30 min. After further cooling down to room temperature for 2 h, the sample was flushed by the Ar stream at room temperature till the stable baseline of GC appeared. Subsequently, TPD measurement was conducted from 293 K to 823 K. (H_2–CO–CO_2)-temperature-programmed surface reaction (TPSR) tests were conducted in a manner similar to that of the H_2-TPD.

3. Results and discussion

3.1. Optimization of catalyst composition

The reaction activity of HAS over a series of Co_3Cu_1–*x*%CNT catalysts with the same Co/Cu molar ratio of 3:1 and varying CNT content was investigated, and the results were shown in Fig. 1. The observed carbon-containing products included C_{1-8}-alcohols, C_{1-4}-hydrocarbons, DME and acetaldehyde (in a small amount), as well as CO_2 (yielded from the water–gas-shift (WGS) side-reaction). The catalyst with 11% of CNT-content showed the highest catalytic activity. The yield of C_{2+}-alc. plus DME (i.e., the product of *X*(CO) and *S*(C_{2+}-alc. + DME), simplified as *Y*(C_{2+}-alc. + DME) in later text) reached 27.5% over this catalyst, while this value of the other four catalysts was successively 24.4%, 23.9%, 21.2%, and 20.1%.

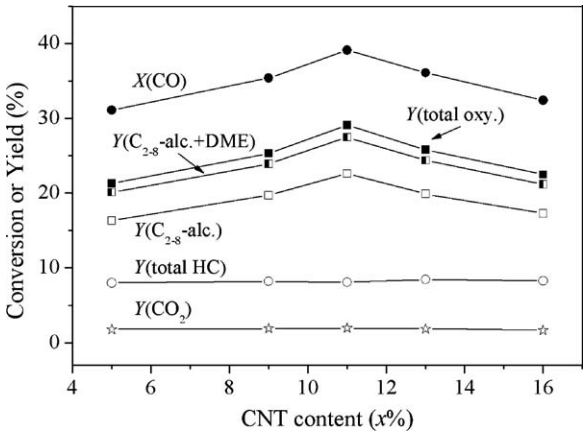

Fig. 1. Reactivity of HAS over Co_3Cu_1–*x*%CNT catalysts with varying CNT content. Reaction conditions: 5.0 MPa, 573 K, $V(H_2)/V(CO)/V(CO_2)/V(N_2) = 45/45/5/5$, GHSV = 7200 ml/(h·g) (inlet).

On the basis of the optimization of CNT content, the dependence of HAS reactivity upon the Co/Cu molar ratio was investigated on a series of Co_iCu_j–11%CNT catalysts with the same CNT content at 11% but varying Co/Cu molar ratio. The results (Fig. 2) showed that the catalyst with the Co/Cu molar ratio of 3:1 had the highest catalytic activity. Over the Co_3Cu_1–11%CNT catalyst, the observed *Y*(total oxy.), *Y*(C_{2-8}-alc. + DME), *Y*(C_{2-8}-alc.), and *Y*(total HC) reached 29.1%, 27.1%, 22.6%, and 8.1%, respectively, under the aforementioned reaction conditions.

3.2. Optimization of reaction conditions

Fig. 3 showed the reactivity of HAS over the Co_3Cu_1–11%CNT catalyst with varying temperatures. With increasing reaction temperature, *X*(CO) increased monotonously, while *Y*(C_{2-8}-alc.) approached a plateau, simultaneously accompanied with accelerated increase of *Y*(total HC) when the temperatures went up to 583 K. In order to obtain high yield of alcohols and low consumption of feed-gas, 573 K was taken as the optimal operating temperature.

It was experimentally found that the presence of a proper amount of CO_2 in the feed-gas over the CNT-promoted Co–Cu system was highly beneficial, instead of harmful, toward hydrogenation–conversion of CO and selective formation of the oxygenated products. As shown in Fig. 4, the syngas doped with 5%CO_2 displayed the highest reactivity. Over the Co_3Cu_1–11%CNT catalyst, addition of 5%CO_2 to the feed-gas led to an increase by 40% in CO-conversion (38.5% vs. 27.1%) under the reaction conditions of 5.0 MPa and 573 K, accompanied with a marked improvement in *S*(total oxy.) and *S*(C_{2-8}-alc.) (74.3% vs. 62.5% and 57.9% vs. 47.5%, respectively) and a certain decrease in *S*(total HC) (20.7% vs. 30.0%).

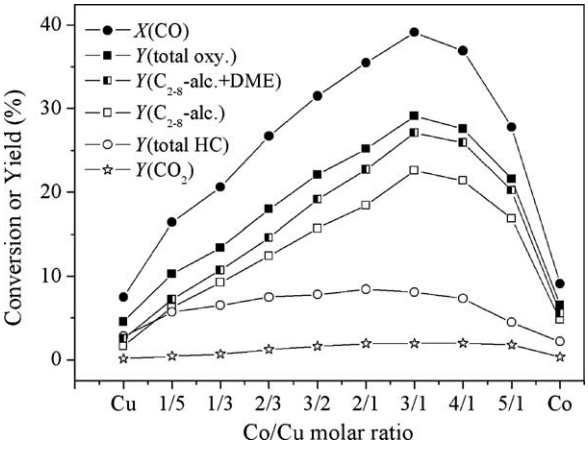

Fig. 2. Reactivity of HAS over Co_iCu_j–11%CNT catalysts with varying Co/Cu molar ratio. Reaction conditions are the same as in Fig. 1.

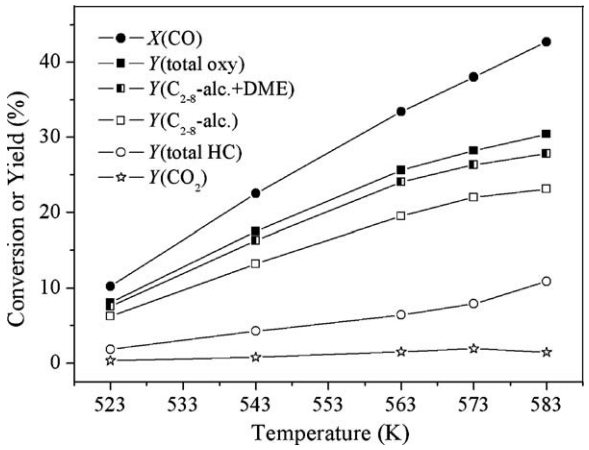

Fig. 3. HAS reactivity over Co_3Cu_1–11%CNT catalyst with varying temperature. Reaction conditions are the same as in Fig. 1 except the reaction temperature.

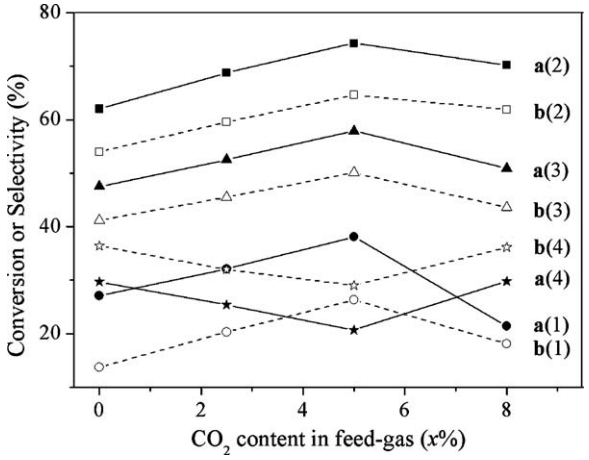

Fig. 4. Effect of CO_2 content in the feed-gas on HAS reactivity over the catalysts: (a) Co_3Cu_1–11%CNT and (b) Co_3Cu_1; (1) *X*(CO), (2) *S*(total oxy.), (3) *S*(C_{2-8}-alc.), and (4) *S*(total HC). Reaction conditions are the same as in Fig. 1 except $V(H_2)/V(CO)/V(CO_2)/V(N_2) = (47.5 - x/2)/(47.5 - x/2)/x/5$.

Effect of H_2/CO molar ratio of the feed-syngas on the reactivity and selectivity of HAS was investigated. The result (see Table 1) showed that over Co_3Cu_1–11%CNT catalyst, the observed single-pass STY of C_{2-8}-alc. plus DME reached 760 mg/(h·g) when fed with the feed-syngas of $H_2/CO = 1$ (molar ratio) (i.e., $V(H_2)/V(CO)/V(CO_2)/V(N_2) = 45/45/5/5$), while merely 441 mg/(h·g) when fed with the feed-syngas of $H_2/CO = 2$ (molar ratio) (i.e., $V(H_2)/V(CO)/V(CO_2)/V(N_2) = 60/30/5/5$). It appears that properly low H_2/CO molar ratio in the feed-syngas is favorable to formation of C_{2-8}-oxygenated products.

3.3. HAS reactivity over the CNT-containing (or free) Co–Cu catalyst

The results of the comparative assay of HAS reaction activity showed that proper incorporation of a minor amount of CNTs into the Co_3Cu_1 host catalyst not only markedly increased the catalyst activity for CO conversion, but also dramatically improved its selectivity for formation of higher alcohols. Under the reaction condition of 5.0 MPa, 573 K, $V(H_2)/V(CO)/V(N_2) = 45/45/10$ and

Table 1
Selectivity and STY of HAS over the Co_3Cu_1–11%CNT catalyst and the related systems.

Catalyst	Feed-gas	CO conv. (%)	Selectivity (C%)					STY (mg/(h·g))			
			Total oxy.	C_{2-8}-alc. + DME	C_{2-8}-alc.	C_{1-4}-HC	CO_2	C_{1-8}-alc. + DME	C_{2-8}-alc. + DME	C_{2-8}-alc.	C_{1-4}-HC
Co_3Cu_1–11%CNT(*h-type*)	(1)	38.3	52.8	47.9	34.8	43.9	3.3	513	441	302	305
	(2)	38.5	74.3	69.3	57.9	20.7	5.0	832	760	611	174
	(3)	27.1	62.5	59.5	47.5	30.0	7.5	501	484	370	187
Co_3Cu_1	(1)	25.9	49.5	45.2	33.9	45.3	5.2	292	253	179	196
	(2)	25.3	64.6	58.7	50.2	29.0	6.4	474	428	341	231
	(3)	13.7	54.1	52.1	41.2	36.4	9.5	228	217	164	115
Co_3Cu_1–11%CNT (*p-type*)	(1)	26.5	49.7	45.6	34.9	45.2	5.1	302	264	192	202
Co_3Cu_1–11%AC	(1)	24.1	49.8	45.8	34.8	44.1	6.1	265	238	172	175

Reaction condition: (1) $V(H_2)/V(CO)/V(CO_2)/V(N_2)$ = 60/30/5/5, GHSV = 7000 ml/(h·g) (outlet); (2) $V(H_2)/V(CO)/V(CO_2)/V(N_2)$ = 45/45/5/5, GHSV = 7200 ml/(h·g) (inlet); (3) $V(H_2)/V(CO)/V(N_2)$ = 45/45/10, GHSV = 7200 ml/(h·g) (inlet); all at 5.0 MPa and 573 K.

GHSV = 7200 ml/(h·g) (inlet), the observed X(CO), S(total oxy.) and S(total HC) were 27.1% vs. 13.7%, 62.5% vs. 54.1% and 30.0% vs. 36.4%, for the Co_3Cu_1–11%CNT vs. the Co_3Cu_1, respectively; while under the reaction condition of 5.0 MPa, 573 K, $V(H_2)/V(CO)/V(CO_2)/V(N_2)$ = 45/45/5/5 and GHSV = 7200 ml/(h·g) (inlet), these values were 38.5% vs. 25.3%, 74.3% vs. 64.6% and 20.7% vs. 29.0%, respectively.

Fig. 5 showed the product distribution of HAS over these catalysts. Over the Co_3Cu_1–11%CNT, the observed $S(C_{2-8}$-alc. + DME) reached 69.3%, which were higher than that (58.7%) of the CNT-free counterpart. The products were the mixtures consisting of linear primary alcohols, hydrocarbons and DME, but the carbon-number distribution of the alcohols and hydrocarbons did not follow the classical Anderson–Schulz–Flory rule. BuOH and DME were the two oxygenate products with the highest carbon-based selectivity, 18.4% and 11.4%, respectively, over the CNT-promoted Co_3Cu_1 catalyst. In comparison, the corresponding numbers were 12.5% and 8.5%, respectively, over the CNT-free counterpart under the same reaction condition.

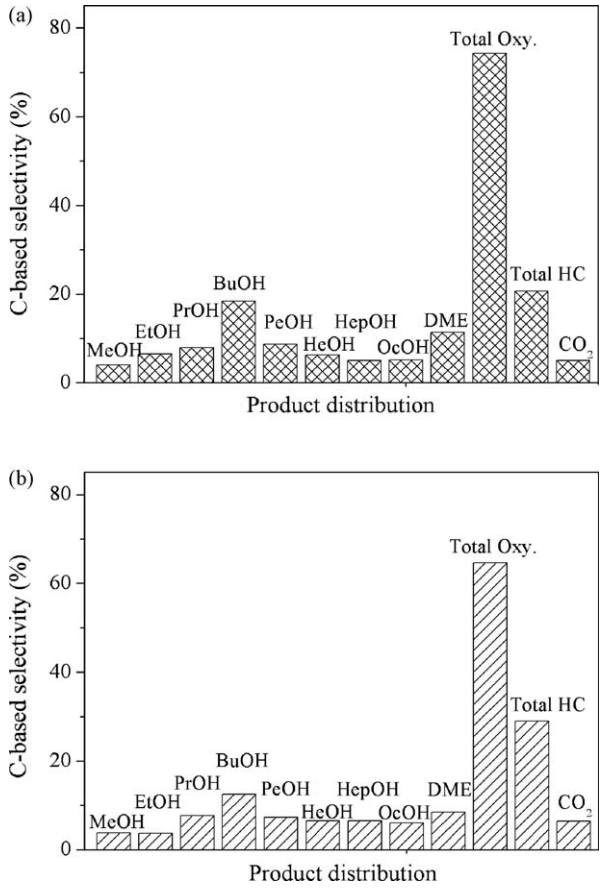

Fig. 5. Product distribution of HAS over the catalysts: (a) Co_3Cu_1–11%CNT and (b) Co_3Cu_1. Reaction conditions are the same as in Fig. 1.

Fig. 6 showed the operation stability of the Co_3Cu_1–11%CNT catalyst for HAS continuing up to 275 h. After 24 h of "running in" stage of the reaction, the catalyst reached a stable operating state, with CO conversion of ~40.0% and selectivity of ~74.7% and ~57.4% for the total oxygenates and C_{2-8}-alcohols, without obvious deactivation observed after 275 h of the reaction.

The single-pass space-time-yields (STYs) of the HAS over the CNT-promoted Co_3Cu_1 catalyst and the related systems were listed in Table 1. Under the reaction condition of 5.0 MPa, 573 K, $H_2/CO/CO_2/N_2$ = 45/45/5/5 (v/v) and GHSV = 7200 ml/(h·g) (inlet), STY of the C_{2-8}-alc. plus DME reached 760 mg/(g·h), being ~78% higher than that (428 mg/(g·h)) of the CNT-free host. The mass% of C_{2-8}-alcohols and DME combined reached ~90% in the total oxygenated products, showing great potential in commercial use for the HAS.

Fig. 7 showed the results of the measurement of apparent activation energy (E_a) of the HAS. The E_a taken on the Co_3Cu_1–11%CNT catalyst was 10.7 kcal/mol (with CO_2-containing feed-gas) or 13.6 kcal/mol (with CO_2-free feed-gas). These values were fairly close to 12.2 kcal/mol taken on the CNT-free host Co_3Cu_1 (with CO_2-containing feed-gas). This indicated that proper incorporation of a minor amount of the CNTs into the Co_3Cu_1 host catalyst did not

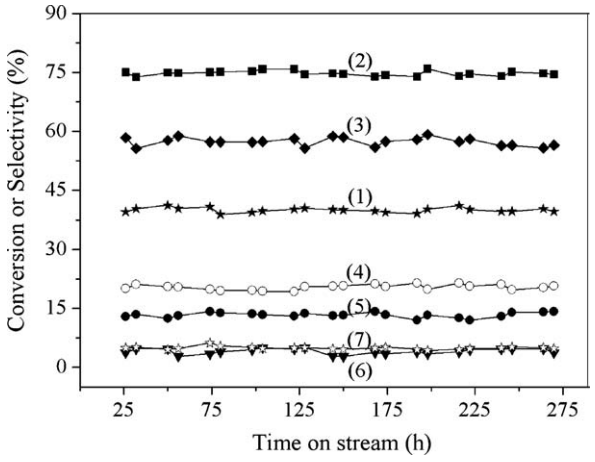

Fig. 6. Operation stability of the Co_3Cu_1–11%CNT catalyst for HAS continuing up to 275 h: (1) X(CO), (2) S(total oxy.), (3) $S(C_{2-8}$-alc.), (4) $S(C_{1-4}$-HC), (5) S(DME), (6) S(MeOH), and (7) $S(CO_2)$. Reaction conditions are the same as in Fig. 1.

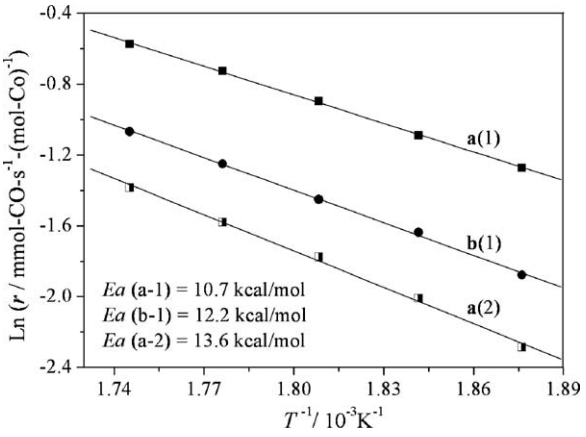

Fig. 7. Arrhenius plots of HAS over the catalysts: (a) Co_3Cu_1–11%CNT and (b) Co_3Cu_1; taken at 2.0 MPa, 523–583 K, with feed-gas: (1) $V(H_2)/V(CO)/V(CO_2)/V(N_2) = 45/45/5/5$ or (2) $V(H_2)/V(CO)/V(N_2) = 45/45/10$, both at GHSV = 12,000 ml/(h·g).

cause a marked change in the E_a for the HAS reaction, most likely implying that the addition of a minor amount of the CNTs to the Co_3Cu_1 did not alter the reaction pathway of rate-determining step of the CO hydrogenation reaction.

3.4. Post-analysis of the tested catalysts by XRD and XPS

The XRD post-analysis of the tested catalysts showed that the XRD pattern of the CNT-containing system were very close to that of the CNT-free host in the position and shape of their XRD features, except the peak at $2\theta = 26.1^\circ$, which was due to diffraction of graphite-like (0 0 2) face of the CNTs [29,30] (see Fig. 8(a) and (b)). This indicated that the addition of a minor amount of the CNTs to the Co_3Cu_1 did not cause a marked change in the phase compositions associated with Co and Cu components. In both catalysts, the Co and Cu components existed mainly in the forms of CoCu-alloy ($2\theta = 44.0^\circ$) and divided copper metal ($2\theta = 51.1^\circ$ and 75.5°), while the content of divided cobalt metal ($2\theta = 41.5^\circ$ and 47.5° for *hcp*-Co_x) was extremely low. According to Scherrer's equation, it could be estimated that the mean particle diameter of CoCu-alloy and copper metal was ~8.4 nm and ~6.2 nm in the CNT-containing catalyst, which were smaller than those (~11.0 nm and ~8.2 nm, respectively) of the CNT-free counterpart, meaning that the CNT-containing catalyst had larger metal surface area.

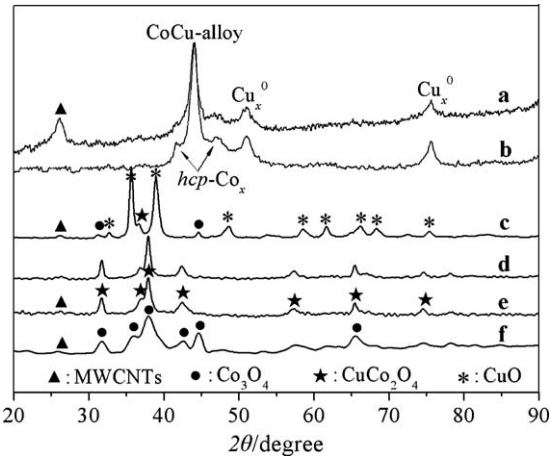

Fig. 8. XRD patterns of the catalysts: (a) Co_3Cu_1–11%CNT (tested); (b) Co_3Cu_1 (tested); (c) Co_1Cu_5–11%CNT (calcined); (d) Co_2Cu_1–11%CNT (calcined); (e) Co_3Cu_1–11%CNT (calcined); (f) Co–11%CNT (calcined).

Fig. 8(c)–(f) showed the XRD patterns of the calcined precursors of four catalysts. The observed main crystallite phase was Co_3O_4 and CuO for the Co–11%CNT (Fig. 8(f)) and Co_1Cu_5–11%CNT (Fig. 8(c)), respectively, while were $CuCo_2O_4$ for Co_2Cu_1–11%CNT (Fig. 8(d)) and Co_3Cu_1–11%CNT (Fig. 8(e)) both. In association with the fact that the latter two catalysts had much higher catalytic activity for HAS, compared to the former two catalysts (see Fig. 2), it could be inferred that it was such a kind of $CuCo_2O_4$ spinel crystallites that would be responsible for generating, through H_2-reduction, the solid–solution-type bimetal Co_iCu_j sites catalytically active for HAS.

Fig. 9(A) showed Cu(2*p*)-XPS spectra of the tested Co_3Cu_1–11%CNT catalyst and the CNT-free counterpart. Little difference in valence of the surface Cu-species existed between the two catalysts. The observed surface Cu-species were all in Cu^0, with $Cu^0(2p_{3/2}) = 932.6$ eV (B.E.) and $Cu^0(2p_{1/2}) = 952.6$ eV (B.E.), indicating that all of the Cu-species at the surface of functioning catalysts existed in the form of metal copper, Cu^0, being in line with the results reported by Sheffer et al. [31].

Unlike the Cu(2*p*)-XPS spectra, remarkable difference in the Co(2*p*)-XPS spectra (Fig. 9(B)) existed between the two tested catalysts. On the CNT-free catalyst (Co_3Cu_1), relatively large amounts of the surface Co-species was in Co^0 [$Co(2p_{3/2}) = 778.0$ eV (B.E.)] and minor in CoO [$Co(2p_{3/2}) = 780.4$ eV (B.E.)] when fed with the CO_2-free feed-gas (Fig. 9(B), b(2)), while

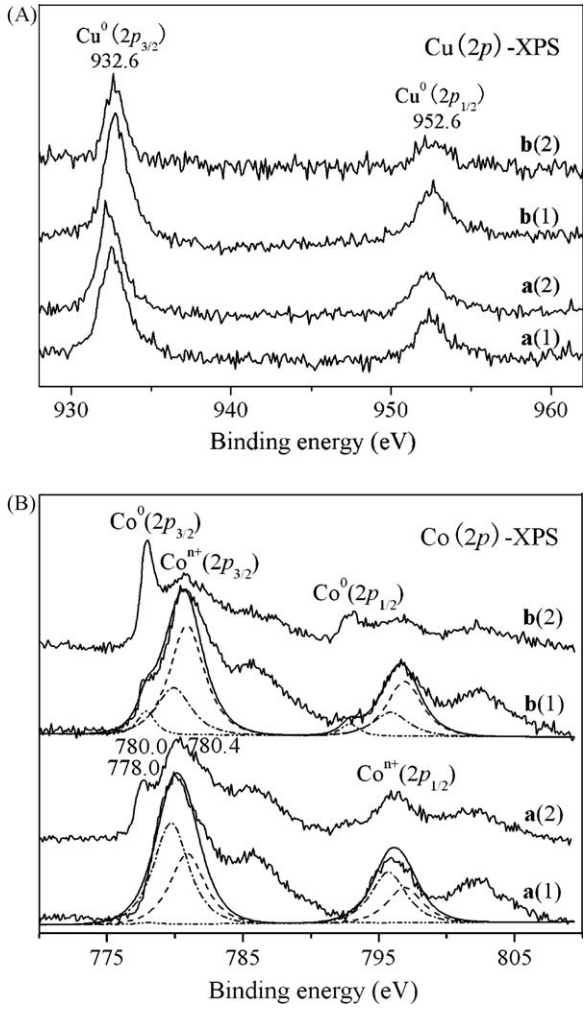

Fig. 9. XPS spectra of Cu(2*p*) (A) and Co(2*p*) (B) of the tested catalysts: (a) Co_3Cu_1–11%CNT and (b) Co_3Cu_1, fed with: (1) the CO_2-containing feed-gas: $V(H_2)/V(CO)/V(CO_2)/V(N_2) = 45/45/5/5$ or (2) the CO_2-free feed-gas: $V(H_2)/V(CO)/V(N_2) = 45/45/10$.

Table 2
Binding energy and relative content (mol%) of different Co-species at the surface of the tested catalysts.

Catalyst	Feed-gas	E_b of Co($2p_{3/2}$) (eV)			Relative content (mol%)		
		Co^0	CoO(OH)	CoO	Co^0	CoO(OH)	CoO
Co_3Cu_1–11%CNT	(1)	778.0	780.0	780.4	0.5	58.8	40.7
	(2)				16.1	51.6	32.3
Co_3Cu_1	(1)	778.0	780.0	780.4	7.0	27.9	65.1
	(2)				39.7	0.7	59.6

Reaction conditions: 5.0 MPa, 573 K, with the feed-gas: (1) $V(H_2)/V(CO)/V(CO_2)/V(N_2)$ = 45/45/5/5 or (2) $V(H_2)/V(CO)/V(N_2)$ = 45/45/10, both at GHSV = 7200 ml/(h·g) (inlet).

dominant amount in CoO and a little in Co^0 when fed with the CO_2-containing feed-gas (Fig. 9(B), b(1)). On the Co_3Cu_1–11%CNT catalyst, in addition to Co^0 and CoO, a type of new Co-species with the Co($2p_{3/2}$) at around 780.0 eV (B.E.) was observed when fed with the CO_2-free feed-gas (Fig. 9 (B), a(2)). This type of Co-species may be ascribed to CoO(OH) [32]. It was particularly interesting that the Co^0 nearly vanished, while the CoO(OH) became the predominant Co-species at the surface of the CNT-containing catalyst fed with the CO_2-containing feed-gas (Fig. 9 (B), a(1)). Analysis and fitting of these Co($2p$)-XPS spectra were carried out and the results (see Table 2) showed that at the surface of the CNT-containing catalyst fed with the CO_2-containing feed-gas, most of the Co-species was CoO(OH), rather than CoO or metallic Co^0. Therefore, it could be suggested that such a kind of surface CoO(OH) species was closely related to the high selectivity of the HAS. It appeared that CO_2 additive in the feed-gas together with the CNT promoter may synergistically play important roles in stabilizing the surface Co-species in the form of CoO(OH), thus increasing the probability of chain termination to form oxygenated products.

3.5. Textural and physico-chemical properties of the CNTs

It was evident that the considerably better performance of the CNT-promoted Co–Cu catalyst for HAS from syngas was closely related to the unique structures and properties of the CNTs used as promoter. The previous HRTEM observation and XRD and Raman measurements have demonstrated that the two kinds of CNTs home-made by catalytic decomposition of CO and CH_4 on a Ni–Mg–O catalyst were a kind of CNTs(*p-type*) and a kind of CNTs(*h-type*), respectively [28–30]. The former is composed of many concentric cylindrical graphene layers placed around a common central hollow. Their surface C-atoms were those located in the facets of the graphene layer, having a higher degree of valence-bond saturation, and thus, fewer dangling bond electrons, resulting in their weak adsorbability towards H_2. Rather different from the former, the latter is constructed by the superposition of many graphene layer facets tilted at a certain angle with respect to the axis of central hollow nanofibre, as if a number of cones were placed one on another. Their surface C-atoms are those at edge of conical graphite-like facets, which are rich in dangling bond electrons. Their degree of valence-bond saturation is relatively low, thus apt to be further saturated by adsorbing some atom, small molecule or group, such as H-atom(s) or -molecule [3].

Fig. 10 showed SEM and HRTEM images of the CH_4-derived CNTs(*h-type*). Their outer diameters were in the range of 10–50 nm and the inner diameters in 3–7 nm, with the N_2-BET specific surface area (SSA) at ~135 m^2/g. The element analysis showed that carbon content in the purified CNTs was ≥99%. The test of temperature-programmed hydrogenation (H_2-TPH, with H_2 of 99.999% purity as reductant) [3,14] showed that the carbon nanostructures in the purified CNTs were predominantly graphite-like (with the TPH peak at around 953 K), and the content of amorphous carbon (with the TPH peak at around 613 K) was very low (less than 10% estimated), and that the temperature needed for initiating the hydrogenation reaction of the CNTs with H_2 was ≥773 K, indicating that this kind of CNTs was stable in H_2-atmosphere at the reaction temperatures for the HAS.

Fig. 11 showed TPD (temperature-programmed desorption) profiles for H_2 adsorbed on the two kinds of CNTs, CNTs(*h-type*) and CNTs(*p-type*) (with the outer diameters of 10–40 nm and the inner diameters of 3–5 nm and the N_2-BET-SSA of ~200 m^2/g), respectively. By combined analysis by GC and MS, it was evidenced that the desorbed product was almost exclusively gaseous hydrogen at temperatures lower than ~693 K. At temperatures higher than ~693 K, the product contained CH_4, C_2H_4 and C_2H_2, in addition to a considerable amount of H_2. This experimental result revealed that H_2 adsorption on these types of CNTs may be in two forms: associative (molecular state) and dissociative (atomic

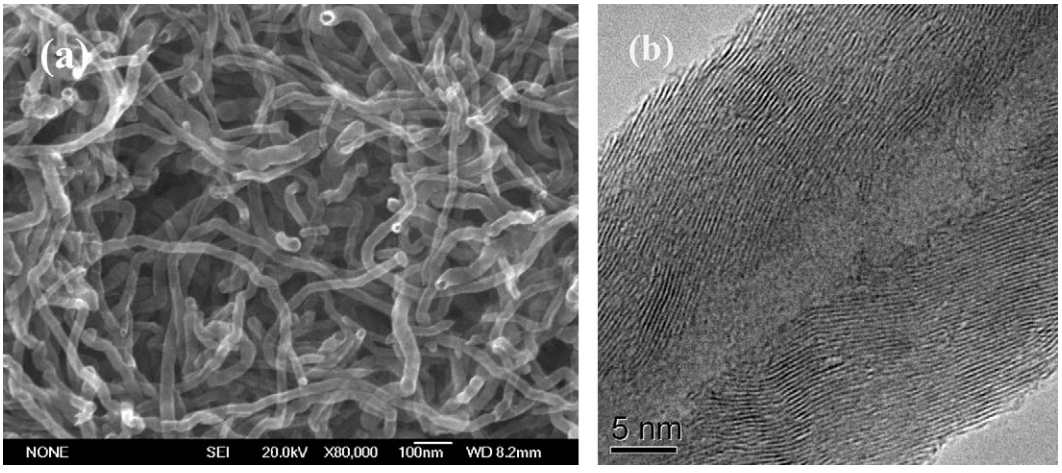

Fig. 10. Images of SEM (a) and HRTEM (b) of the purified CNTs(*h-type*).

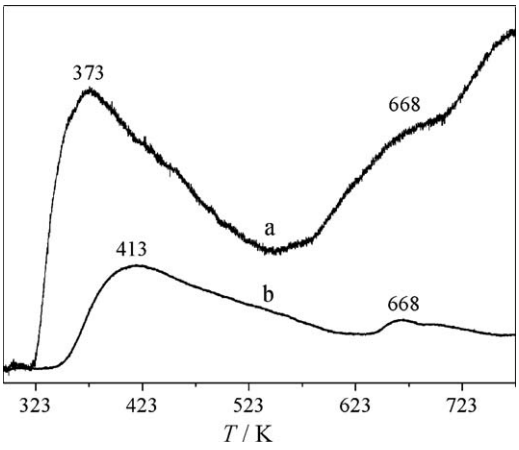

Fig. 11. TPD profiles of hydrogen adsorption on: (a) CNTs(*h-type*) and (b) CNTs(*p-type*), at room temperature.

state). Moreover, it was evident that the hydrogen adsorption capacity of the CNTs(*h-type*) was considerably higher than that of the the CNTs(*p-type*). These were in good agreement with the aforementioned results of Raman characterization of the H_2/CNTs adsorption systems [30,33].

3.6. TPD/TPSR characterization of the pre-reduced catalysts

H_2-TPD measurements also provided useful information about hydrogen ad-species and their relative concentrations at the surface of catalysts. The solid lines in Fig. 12 showed the TPD profiles taken on the pre-reduced catalysts adsorbing H_2 (99.999% purity) at 433 K followed by cooling down to room temperature. On the CNT-free catalyst, Co_3Cu_1, desorption of H-adspecies started at 333 K, approached a peak at 410 K, and ended at 523 K; while on the Co_3Cu_1–11%CNT(*h-type*) catalyst, a shoulder-peak (region-II) spanning from 473 K to 623 K, which resulted from the desorption of H-species chemisorbed strongly, was observed, in addition to a main peak (region-I) at 418 K due to desorption of weakly adsorbed H-species. It could be estimated that total area-intensity of the TPD-profile (corresponding to a certain H_2-desorbed amount) taken on the CNT(*h-type*)-containing system in the range of 333–623 K was 2.5 times that of the CNT-free system. It was conceivable that, at the reaction temperatures for HAS (523–583 K for the present work), the surface concentration of the kind of H-adspecies interrelated with region-I (spanning from 333 K to 473 K) was expected to be extremely low, and most of H-adspecies at the surface of functioning catalysts was those interrelated to region-II (spanning from 473 K to 623 K). Therefore, it could be inferred that the kind of H-adspecies interrelated with region-II was closely associated with the reaction activity of HAS. The relative area-intensity ratio of the region-II for the two catalysts was estimated to be: (Co_3Cu_1–11%CNT):(Co_3Cu_1) = 5.6:1. This suggested that the sequence of increasing surface concentration of H-adspecies on the functioning catalysts was (Co_3Cu_1–11%CNT) > (Co_3Cu_1), in line with the observed sequence of reaction activity of HAS over these catalysts.

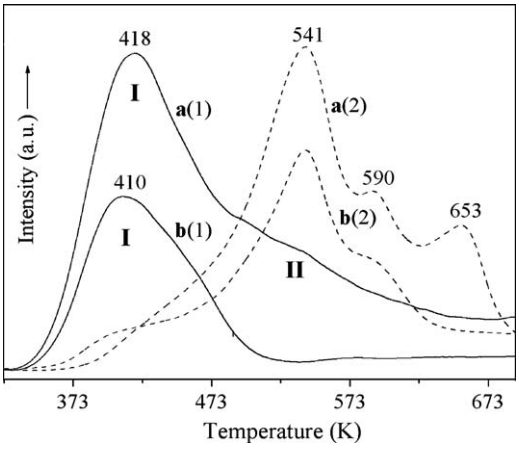

Fig. 12. H_2-TPD (1) and (H_2–CO–CO_2)-TPSR (2) profiles of the pre-reduced catalysts: (a) Co_3Cu_1–11%CNT and (b) Co_3Cu_1.

Using the feed-gas of $V(H_2)/V(CO)/V(CO_2)$ = 45/45/5 in place of H_2 as adsorbate in the above experiments, the observed TPD–TPSR (temperature-programmed surface reaction) profiles were shown by the dashed lines in Fig. 12. On the Co_3Cu_1–11%CNT sample pre-adsorbing the feed-gas of H_2/CO/CO_2, a main peak at 541 K and two shoulder-peaks at 590 K and 653 K were observed. The desorbed product was mainly H_2 and CO at temperatures below 523 K, and contained C_{1-8}-oxygenates and C_{1-4}-hydrocarbons in addition to H_2 and CO at temperatures of 523 K and above. With temperature increasing and the surface reaction accelerating, most of adspecies of H_2, CO and CO_2 remaining at the surface may be converted to the products of HAS, followed by the latter's desorption, so that the whole process of TPD–TPSR came to an end with temperature running up to ~693 K. Similar TPD–TPSR behavior was also observed on the CNT-free counterpart, but its adsorption capacity for the feed-syngas of H_2/CO/CO_2 was relatively low. The observed sequence of adsorption capacity of the two catalysts toward the feed-gas of H_2/CO/CO_2 was Co_3Cu_1–11%CNT > Co_3Cu_1, again in line with the observed sequence of reaction activity of HAS over these catalysts.

3.7. Nature of the CNT-promoter action

The aforementioned results of the catalyst evaluation showed that appropriate incorporation of a minor amount of the CNTs into the Co_3Cu_1 host catalyst led to a significant increase in CO conversion and selectivity for the higher alcohols. Yet the result of measurement of apparent activation energy (E_a) indicated that the addition of a minor amount of the CNTs into the Co_3Cu_1 host catalyst did not cause a marked change in the E_a for the HAS, most likely implying that the addition of a minor amount of the CNTs to the Co_3Cu_1 did not alter the reaction pathway of rate-determining step of the CO hydrogenation reaction.

The measurements of the amount of CO adsorbed on the H_2-reduced catalyst samples could provide the valuable information about active metal surface area. Unfortunately, since metallic Co and Cu both can adsorb CO in varying degrees and they may have different CO-site occupation sequence and adsorption model [34,35], it is impossible to calculate a definite active metal surface area from the amount of CO adsorbed on these CoCu-based catalysts. Still, the relative ratio of the active metal surface areas of different catalyst samples could be estimated. Such experiments have been done, and the results showed that under the condition of 298 K and 0.1 MPa, the amount of CO chemisorbed on the H_2-reduced Co_3Cu_1–11%CNT sample was 1.21 times that of the H_2-reduced Co_3Cu_1 host. This suggested that the active metal surface area of the Co_3Cu_1–11%CNT catalyst was about 1.21 times that of the CNT-free Co_3Cu_1. The increase of the N_2-BET-SSA (120.2 (calcined) and 68.8 (tested) m^2/g for the Co_3Cu_1–11%CNT; 108.2 (calcined) and 53.3 (tested) m^2/g for the Co_3Cu_1), especially the active metal surface area, was undoubtedly in favor of enhancing the specific activity of the catalyst (i.e., activity of unit mass of catalyst). Nevertheless, it would be difficult to believe that the increase of as high as 50% in CO conversion (i.e., 38.5% vs. 25.3% for the Co_3Cu_1–11%CNT vs. the Co_3Cu_1, see Table 1) was solely

attributed to the difference in their SSA or active metal surface area.

In recent years there has been considerable experimental and theoretical interest in the use of nanostructured carbon materials as potential hydrogen sorbents. It was demonstrated by Ishikawa et al. [36] that graphitized carbon black surfaces were capable of rapidly equilibrating H_2/D_2 mixture. A dissociation rate of 2.5×10^{17} molecules s^{-1} $(m^2\text{-ASA})^{-1}$ (ASA—active surface area) was measured at ambient temperatures and pressures, regardless of the nature of the carbon material under investigation. The ASA was described in terms of atoms located at edge positions on the graphite basal plane and was determined from the amount of oxygen able to chemisorb at these sites.

It appears that the high reactivity of HAS over the CNT(*h-type*)-promoted Co_3Cu_1 catalyst was closely related to the peculiar properties of this kind of CNTs, especially their excellent performance for adsorption/activation of H_2. Based upon the above TPD results, it could be suggested that, under the reaction conditions of the HAS, there existed a considerably larger amount of reversibly adsorbed H-species on the CNT(*h-type*)-promoted Co_3Cu_1 catalyst, which would generate a surface micro-environment with high stationary-state concentration of H-adspecies on the catalyst. Those active H-adspecies could be readily transferred to Co_iCu_j active sites via the CNT-promoted hydrogen spillover, thus increase the rate of a series of surface hydrogenation reactions in the HAS. This was very similar to the cases of methanol synthesis over the CNT-supported/promoted Cu–Zn–Al catalysts [12,13] and HAS over the Co-decorated CNT-promoted Co–Mo–K catalyst [17]. Alternatively, synergistic action of the high surface-concentration H-adspecies with CO_2 in the feed-gas led to a significant increase of the surface concentration of the CoO(OH)-species (a kind of catalytically active Co-species closely associated with the alcohols generation) on one hand, and a greater inhibition for the water–gas-shift side-reaction on the other hand. All these factors contributed considerably to an increase in the yield of alcohols. Compared to the CNTs(*h-type*), the CNTs(*p-type*)'s capacity for adsorption and activation of H_2 was much lower, and thus, its promoter action was not marked. In sharp contrast to the CNTs(*h-type*)-doped catalyst, doping of the AC (activated carbon, a kind of amorphous carbon, Xiamen Chem. Reagent Co., with 830 m^2/g of N_2-BET-SSA) into the Co_3Cu_1 host catalyst not only was unhelpful to improving the performance of the catalyst, but also led to a certain decrease in conversion of CO and STY of (C_{1-8}-alc. + DME) (see Table 1).

4. Conclusion

The present work showed that CNTs(*h-type*) could serve as an excellent catalyst-promoter for CO/CO_2 hydrogenation reactions. The CNT(*h-type*)-promoted Co_3Cu_1 catalyst achieved highly selective formation of C_{2-8}-oxygenates, especially BuOH and DME, from syngas, and demonstrated great potential in commercial use for the HAS. The results also shed some light on the understanding of the promoter action by the CNT additive and on the design of catalyst for the HAS. For better understanding of mechanism of the promoter action by the CNTs, further studies, especially *in situ* characterization of reaction intermediates under the HAS reaction condition, would be desirable.

Acknowledgments

The authors are grateful for the financial supports from the National Natural Science Foundation Project (No. 20590364), National "973" Projects (No. 2005CB221403) and (No. 2009CB939804) of China.

References

[1] K.P. de Jong, J.W. Geus, Catal. Rev. Sci. Eng. 42 (2000) 481.
[2] P. Serp, M. Corrias, P. Kalck, Appl. Catal. A: Gen. 253 (2003) 337.
[3] H.-B. Zhang, G.-D. Lin, Y.-Z. Yuan, Curr. Top. Catal. 4 (2005) 1.
[4] S. Iijima, Nature 354 (1991) 56.
[5] J.M. Planeix, N. Coustel, B. Coq, V. Brotons, P.S. Kumbhar, R. Dutartre, P. Geneste, P. Bernier, P.M. Ajiayan, J. Am. Chem. Soc. 116 (1994) 7935.
[6] M.S. Hoogenraad, M.F. Onwezen, A.J. van Dillen, J.W. Geus, Stud. Surf. Sci. Catal. 101 (1996) 1331.
[7] Y. Zhang, H.-B. Zhang, G.-D. Lin, P. Chen, Y.-Z. Yuan, K.-R. Tsai, Appl. Catal. A: Gen. 187 (1999) 213.
[8] Z.-J. Liu, Z.-D. Xu, Z.-Y. Yuan, D.-Y. Lu, W.-X. Chen, W.-Z. Zhou, Catal. Lett. 72 (2001) 203.
[9] C.-B. Li, W.-X. Pan, W.-K. Wong, J.-L. Li, X.-Q. Qiu, X.-P. Chen, J. Mol. Catal. A: Chem. 193 (2003) 71.
[10] H.-B. Chen, J.-D. Lin, Y. Cai, X.-Y. Wang, J. Yi, J. Wang, G. Wei, Y.-Z. Lin, D.-W. Liao, Appl. Surf. Sci. 180 (2001) 328.
[11] E. van Steen, F.F. Prinsloo, Catal. Today 71 (2002) 327.
[12] H.-B. Zhang, X. Dong, G.-D. Lin, Y.-Z. Yuan, P. Zhang, K.-R. Tsai, in: C.J. Liu, R.G. Mallinson, M. Aresta (Eds.), Utilization of Greenhouse Gases, ACS Symp. Ser, 852, American Chemical Society, Washington, DC, 2003, p. 195.
[13] X. Dong, H.-B. Zhang, G.-D. Lin, Y.-Z. Yuan, K.-R. Tsai, Catal. Lett. 85 (2003) 237.
[14] H.-B. Zhang, X. Dong, G.-D. Lin, X.-L. Liang, H.-Y. Li, Chem. Commun. (2005) 5094.
[15] H.-B. Zhang, X. Dong, G.-D. Lin, X.-L. Liang, Y.-T. Guo, P. Zhang, in: Proceedings of the 232nd ACS National Meetings, Fuel Chemistry Division, San Francisco, 2006, Paper No. 244 (Oral)..
[16] X.-M. Ma, G.-D. Lin, H.-B. Zhang, Catal. Lett. 111 (2006) 141.
[17] X.-M. Wu, Y.-Y. Guo, J.-M. Zhou, G.-D. Lin, X. Dong, H.-B. Zhang, Appl. Catal. A: Gen. 340 (2008) 87.
[18] R.R. Chianelli, J.E. Lyons, G.A. Mills, Catal. Today 22 (1994) 361.
[19] P. Courty, D. Durand, E. Freund, A. Sugier, J. Mol. Catal. 17 (1982) 241.
[20] A. Razzaghi, J.P. Hindermann, A. Kiennemann, Appl. Catal. 13 (1984) 193.
[21] A. Kiennemann, C. Diagne, J.P. Hindermann, P. Chaumette, P. Courty, Appl. Catal. 53 (1989) 197.
[22] A. Kiennemann, S. Boujana, C. Diagne, P. Chaumette, Stud. Surf. Sci. Catal. 75 (1993) 1479.
[23] R.G. Herman, Stud. Surf. Sci. Catal. 64 (1991) 266.
[24] P. Forzatti, E. Tronconi, I. Pasquon, Catal. Rev. Sci. Eng. 33 (1991) 109.
[25] A.B. Stiles, F. Chen, J.B. Harrison, X. Hu, D.A. Storm, H.X. Yang, Ind. Eng. Chem. Res. 30 (1991) 811.
[26] J.C. Slaa, J.G. van Ommen, J.R.H. Ross, Catal. Today 15 (1992) 129.
[27] K.A.N. Verkerk, B. Jaeger, C.H. Finkeldei, W. Keim, Appl. Catal. A: Gen. 186 (1999) 407.
[28] P. Chen, H.-B. Zhang, G.-D. Lin, Q. Hong, K.-R. Tsai, Carbon 35 (1997) 1495.
[29] P. Chen, H.-B. Zhang, G.-D. Lin, K.-R. Tsai, Chem. J. Chin. Univ. 19 (1998) 765.
[30] H.-B. Zhang, G.-D. Lin, Z.-H. Zhou, X. Dong, T. Chen, Carbon 40 (2002) 2429.
[31] G.R. Sheffer, R.A. Jacobson, T.S. King, J. Catal. 116 (1989) 95.
[32] J.F. Moulder, W.F. Stickle, P.E. Sobol, K.D. Bomben, Handbook of X-ray Photoelectron Spectroscopy—A Reference Book of Standard Spectra for Identification and Interpretation of XPS data, Physical Electronics Inc., Eden Prairie, MN, USA, 1995
[33] Z.-H. Zhou, X.-M. Wu, Y. Wang, G.-D. Lin, H.-B. Zhang, Acta Phys. Chim. Sin. 18 (2002) 692.
[34] M. Kiskinova, Stud. Surf. Sci. Catal. 64 (1991) 37.
[35] V. Ponec, Stud. Surf. Sci. Catal. 64 (1991) 117.
[36] Y. Ishikawa, L.G. Austin, D.E. Brown, P.L. Walker Jr., Chemistry and physics of carbon, in: P.L. Walker, Jr., P.A. Thrower (Eds.), American Carbon Society, vol. 12, Marcel Dekker, New York, 1975, p. 39.